Nanoparticles in Biology

DOI: 10.1002/anie.201101499

Selective Targeting of Fluorescent Nanoparticles to Proteins Inside Live Cells**

*Domenik Liße, Verena Wilkens, Changjiang You, Karin Busch, and Jacob Piehler**

Single-molecule localization and tracking techniques have contributed towards observing the spatiotemporal organization of proteins in the plasma membrane.[1,2] Individual proteins labeled with fluorescent nanoparticles (FNPs) can be imaged over long time with ultrahigh spatial and temporal resolution.[3–8] A key challenge for the biophysical application of FNPs, however, is to site-specifically target the nanoparticles to proteins in living cells. For selective labeling of cell surface proteins with FNPs, biomolecules such as antibodies and streptavidin have been employed as well as chemical recognition based on immobilized transition-metal ions.[5,8–12] These recognition units, however, are not compatible with FNP targeting to proteins inside living cells, because the structural integrity of antibodies is often affected by the reducing conditions in the cytoplasm, streptavidin is blocked with endogenous biotin, and transition-metal ions are coordinated by cysteine-rich proteins. Intracellular FNP targeting is furthermore challenging, because blocking of nonspecific binding and washing out of nonbound FNPs is not possible in intact cells. Here, we aimed to establish a highly specific and efficient approach for FNP targeting inside live cells, which overcomes these particular challenges. As a biochemical recognition system compatible with the cytoplasm, we employed an enzymatic covalent labeling approach based on the HaloTag. This engineered dehalogenase irreversibly reacts with a chlorohexane moiety (HaloTag ligand, HTL) attached to fluorescent dyes and other probes. This highly specific reaction has been exploited for protein labeling in live cells.[13,14]

We attempted functionalization of FNPs with HTL through maleimide/thiol-chemistry as well as by using different biotin derivatives. However, neither significant specific binding to the immobilized HaloTag was observed in vitro, nor efficient targeting upon microinjection into live cells expressing HaloTag fusion proteins using a microcapillary. For this reason, we characterized the association kinetics of different derivatives of the HTL in more detail using real-time surface-sensitive detection by simultaneous reflectance interference (RIF) and total internal reflection fluorescence spectroscopy (TIRFS) detection.[15]

For this purpose, purified HaloTag with a His-tag (His = histidine, HaloTag-H12) was site-specifically immobilized on a polyethylene glycol (PEG) polymer brush functionalized with tris(nitrilotriacetic acid), tris-NTA,[16] and binding of fluorescent substrates was monitored in real time (see Figure S1 in the Supporting Information). Rapid binding of HTL conjugated with the fluorescent dye AlexaFluor 488 (^{AF488}HTL) was detected by TIRFS (see Figure S1 in the Supporting Information), yielding a reaction rate constant of $1\times10^{5}\,M^{-1}s^{-1}$. To directly compare the reaction rate constants of fluorescent and nonfluorescent HTL conjugates (see Scheme S1 in the Supporting Information), a competition assay was established with ^{AF488}HTL as a fluorescent tracer (see Figure S2 in the Supporting Information). These rate constants are summarized in Table S1 in the Supporting Information. Strikingly, a substantially faster reaction rate constant of $1\times10^{6}\,M^{-1}s^{-1}$ was observed for HTL conjugated with tetramethylrhodamine (^{TMR}HTL), which is similar to the published rate constant of this reaction measured in solution ($2.7\times10^{6}\,M^{-1}s^{-1}$).[13] Surprisingly, an elongated ethylene glycol linker substantially reduced the reaction rate constant. Even slower rate constants were obtained for biotinylated and for unmodified HTL (around $10^{3}\,M^{-1}s^{-1}$). These results suggested that the conjugated fluorescence dyes play a critical role for the association kinetics, probably by stabilizing the non-covalent enzyme–substrate complex, by hydrophobic interactions, prior to the ester formation by reaction with D106 in the binding pocket of the HaloTag. Strikingly, engineering of the HaloTag from the original dehalogenase involved incorporation of hydrophobic residues in the proximity of the reactive site.[13]

Based on the observation that hydrophobic as well as positively charged residues increase the reaction rate constant of HTL derivatives, we implemented a novel approach for surface functionalization with the HTL based on click chemistry using commercially available dibenzocyclooctyne-like (DBCO) derivatives and azide-functionalized HTL (Figure 1a and Scheme S2 in the Supporting Information). Thus a hydrophobic moiety was integrated to HTL similar to the HTL-dye conjugates. The reaction kinetics of the HTL derivative obtained by this reaction (clickHTL) was compared with other HTL-derivatives of the competitive binding

[*] D. Liße, Dr. C. You, Prof. Dr. J. Piehler
Division of Biophysics, Department of Biology
Universität Osnabrück, Barbarastrasse 11
49076 Osnabrück (Germany)
E-mail: piehler@uos.de
Homepage: http://www.biologie.uni-osnabrueck.de/Biophysik/Piehler/

V. Wilkens, Prof. Dr. K. Busch
Mitochondrial Dynamics, Department of Biology
Universität Osnabrück, Barbarastrasse 11
49076 Osnabrück (Germany)

[**] We thank Gabriele Hikade, Hella Kenneweg, and Wladislaw Kohl for technical assistance, and Roland Wedlich-Söldner for providing the Lifeact plasmid. This project was supported by the DFG (grant numbers PI405-4 and BU2288-1) and by the Human Frontier Program Organization (grant number RGP 5/2007).

Supporting information for this article is available on the WWW under http://dx.doi.org/10.1002/anie.201101499.

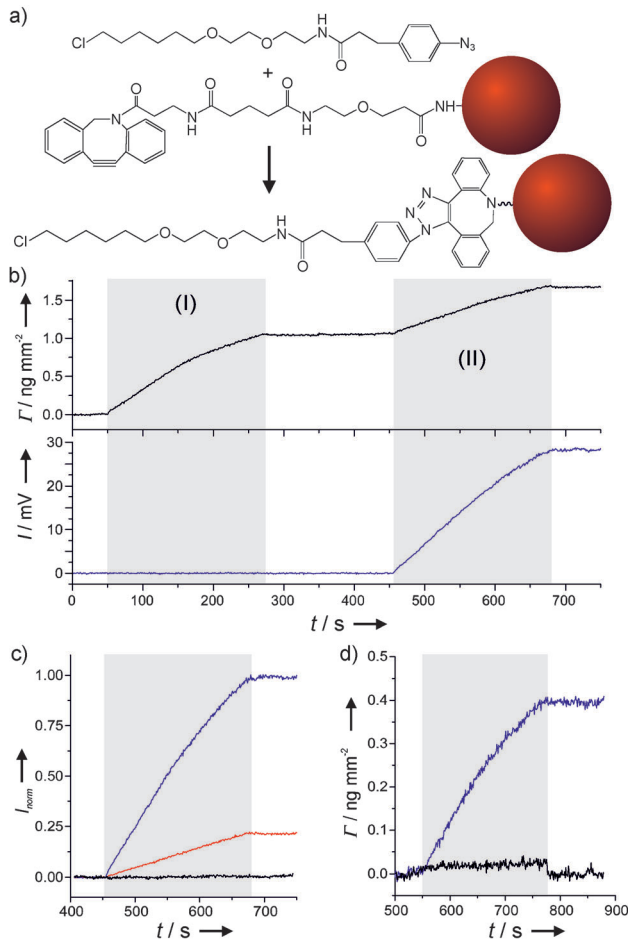

Figure 1. Fast-associating HaloTag ligand (HTL) derivative for nanoparticle functionalization. a) HTL derivative for coupling to surfaces by click chemistry. b) Immobilization of the HaloTag-H12 (I) and binding of fluorescent nanoparticles (FNPs, 50 nM) functionalized with clickHTL (II) as monitored by reflectance interference (RIF, top) and total internal reflection fluorescence spectroscopy (TIRFS, bottom). c) Binding of FNPs (50 nM) functionalized with clickHTL (blue) and with HTL-thiol (red) compared to nonfunctionalized FNPs. Relative binding signals normalized with respect to the amount of immobilized HaloTag are compared. d) Binding of EGFP-HaloTag (1 μM) to immobilized FNP functionalized with clickHTL (blue). As a control, binding to nonfunctionalized FNP is shown (black). The gray areas mark the injection periods.

assay (see Figure S3 in the Supporting Information). An arround 10-fold faster reaction compared to that of HTL-thiol was observed, with an estimated rate constant of around $4 \times 10^4\,\text{M}^{-1}\,\text{s}^{-1}$.

This improved HTL was further employed for FNP functionalization. For commercially available quantums dots, nonspecific binding to intracellular membranes was observed upon prolonged incubation. For this reason, we used amine-functionalized polystyrene FNPs loaded with rhodamine B with an average hydrodynamic diameter of 20 nm (see Figure S4 in the Supporting Information) and a ζ-potential of (-26.7 ± 3.6) mV. These FNPs were conjugated with clickHTL as outlined in Figure 1a. The average degree of functionalization (DOF) was estimated based on the absorbance of DBCO before and after the click reaction (see Figure S5 in the Supporting Information). Depending on the concentration of NHS-DBCO, FNPs with DOFs between around 2 and 10 clickHTL units were synthesized. The average number of binding sites per FNP was determined after reaction with the purified HaloTag fused to EGFP (HaloTag-EGFP) by using analytical size exclusion chromatography (see Figure S6 in the Supporting Information). Thus, the reactivity of the HTL on the NP surface was confirmed. Moreover, we monitored the reaction of clickHTL-functionalized FNPs (clickHTL-FNP) with immobilized HaloTag by simultaneous TIRFS-RIF detection (Figure 1b). Fast and specific binding to the surface was observed, while a much slower reaction was observed for FNPs functionalized with HTL-thiol (Figure 1c).

We also probed the kinetics of the HaloTag reacting with clickHTL on the surface of the FNPs, which was immobilized on the transducer surface through additional biotin moieties. Specific reaction of HaloTag-EGFP was observed by RIF and TIRFS detection (Figure 1d), yielding reaction rates of $4 \times 10^3\,\text{M}^{-1}\,\text{s}^{-1}$. In contrast, binding of HaloTag-EGFP was hardly

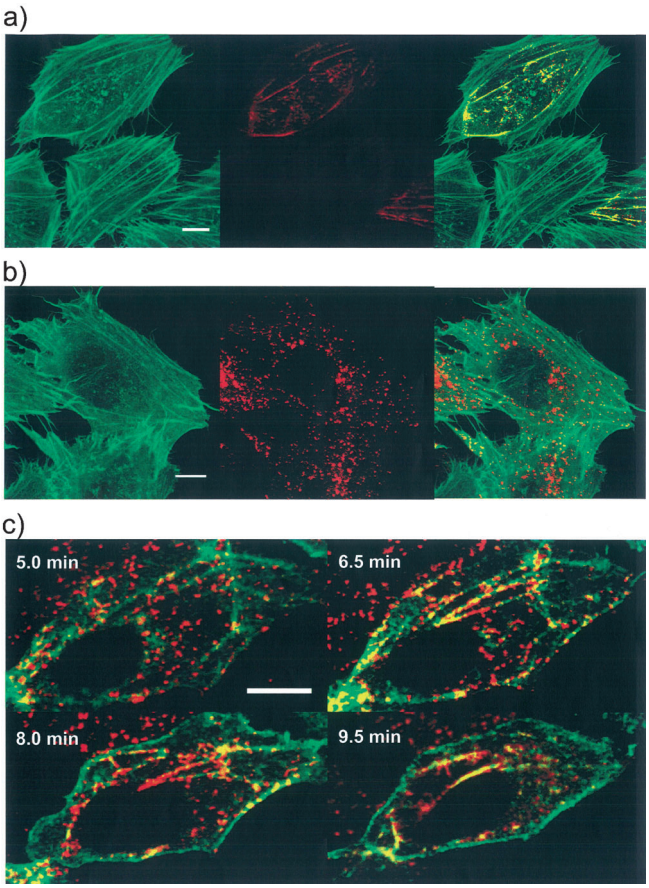

Figure 2. Specific targeting of clickHTL-FNPs to the cytoskeleton. a) Confocal images of HeLa cells stably transfected with Lifeact-EGFP-HaloTag (EGFP = enhanced green fluorescent protein) 1 h after injection of clickHTL-FNP (left: GFP channel; center: FNP channel; right: overlay). b) Control experiment with DBCO-functionalized (DBCO = dibenzocyclooctyne) FNPs injected into the same HeLa cell line. c) Time-lapse imaging of clickHTL FNP binding to the cytoskeleton. The scale bar corresponds to 10 μm in all panels.

detectable for FNPs functionalized with HTL-thiol. These measurements suggest that the reaction rate constant for the HTL derivatives are substantially reduced upon immobilization on solid supports.

To test specific targeting to proteins in the cytoplasm of living cells, clickHTL-FNP with a DOF of 10 were microinjected into HeLa cells stably transfected with Lifeact fused to both EGFP and the HaloTag (Lifeact-EGFP-HaloTag). Lifeact is a 17 amino acid peptide, which reversibly binds to the actin cytoskeleton.[17] After 1 h of injection high co-localization of the clickHTL-FNP with the actin filaments stained by Lifeact-EGFP-HaloTag was observed (Figure 2a). More than 90% of the FNP co-localized with the EGFP signal. In contrast, a random distribution of FNPs functionalized with DBCO solely was observed upon injection into the same cell line (Figure 2b and Figure S7 in the Supporting Information). In cells expressing Lifeact-EGFP-HaloTag, time-lapse dual color confocal imaging confirmed rapid binding of clickHTL-FNPs to the cytoskeleton within 10 min (Figure 2c and Video 1 in the Supporting Information). In contrast, no significant co-localization was observed for FNPs directly functionalized with HTL under the same conditions (data not shown), supporting that a more efficient reaction is required for intracellular targeting. For exploring FNPs targeting to membrane proteins inside living cells, we fused the HaloTag to TOM20, a subunit of the translocase in the outer membrane (TOM) of mitochondria. ClickHTL-FNPs with a DOF of 5 injected into HeLa cells stably expressing TOM20-EGFP-HaloTag specifically co-localized with mitochondria (Figure 3a). In a negative control experiment no significant co-localization of clickHTL-FNP with the mitochondria was observed in HeLa cells stably expressing respiratory chain complex III in the inner mitochondrial membrane fused to EGFP (CIII-EGFP, Figure 3c and Video 2 in the Supporting Information), confirming that highly specific intracellular FNP targeting to intracellular membrane proteins was possible by this method. However, cross-linking of mitochondria by the clickHTL-FNPs was observed as well as a very low mobility of these FNPs, which can be ascribed to the multivalent functionalization. In contrast, a much higher mobility of the FNPs was observed in the negative control experiment (see Figure S8 and Video 2 in the Supporting Information). The high mobility of free FNPs is responsible for their blurred appearance under long exposure times used for confocal imaging (Figure 3b,c).

To employ this labeling approach for tracking molecules within live cells, we functionalized FNPs with clickHTL at a very low degree of functionalization (average DOF of 0.7 clickHTL moieties per FNP). After injection of these clickHTL-FNPs into cells transfected with TOM20-EGFP-HaloTag, a substantial fraction of the FNPs co-localized over extended times with mitochondria (Figure 4a and Video 3 in the Supporting Information). As expected, a substantially higher mobility of these FNPs along the mitochondria was observed compared to the higher functionalized FNPs used for co-localization experiments before. Moreover, the mito-

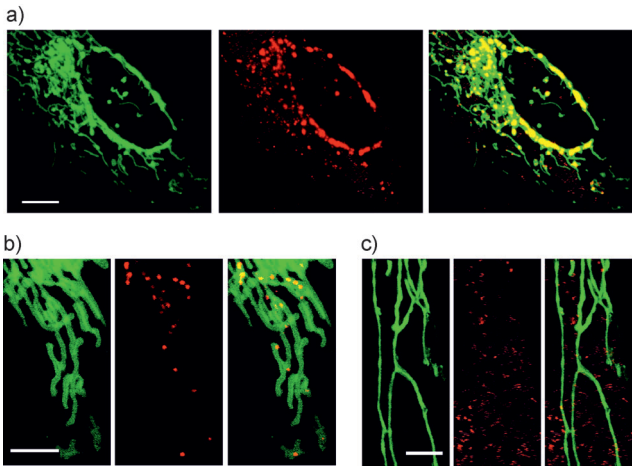

Figure 3. Labeling of a mitochondrial outer membrane protein with clickHTL-FNPs. a) Confocal images of HeLa cells stably transfected with TOM20-EGFP-HaloTag after microinjection of clickHTL-FNP (TOM20 = subunit of the translocase in the outer membrane of mitochondria). The scale bar corresponds to 10 µm. b) Detailed view of mitochondria with TOM20-EGFP-HaloTag labeled with clickHTL-FNPs. c) Detailed view of mitochondria in negative control cells transfected with inner mitochondrial membrane protein CIII-EGFP. The scale bars in panels (b) and (c) correspond to 5 µm.

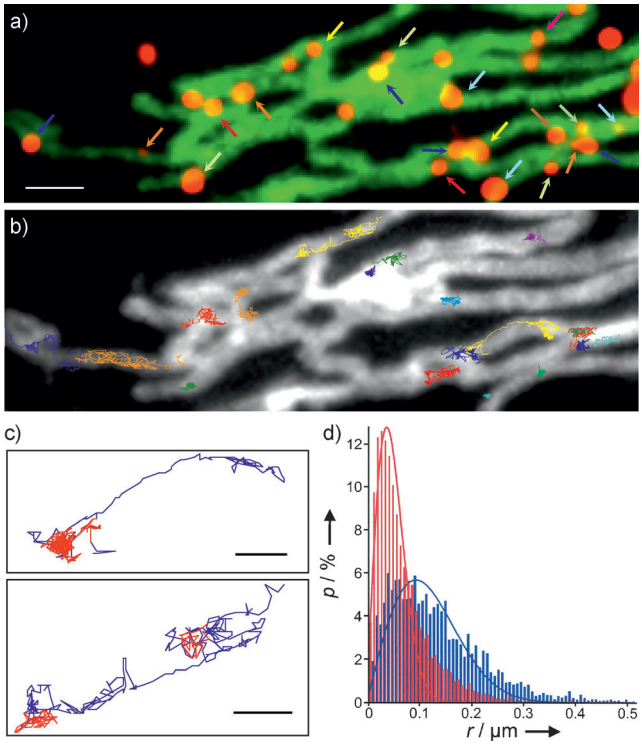

Figure 4. Tracking single FNPs bound to TOM20. ClickHTL-FNPs with a very low degree of functionalization (DOF) were injected into HeLa cells stably transfected with TOM20-EGFP-HaloTag. a) Single overlay image of the GFP and the FNP channels from a stack of 500 camera frames (HILO mode imaging). The scale bar corresponds to 2 µm. FNPs marked with arrows remained associated to individual mitochondria over 500 frames. b) Trajectories for individual clickHTL-FNPs indicated by arrows in panel (a) (corresponding color coding). c) Selected trajectories analyzed for transient confinement zones, which are depicted in red. The scale bar corresponds to 500 nm. d) Cumulative step length analysis for diffusion within (red) and outside (blue) transient confinement zones.

chondrial network was much less perturbed by these FNPs. Thus, tracking of individual FNPs diffusing along mitochondria was possible. Trajectories obtained by this approach nicely followed the shape of the mitochondria (Figure 4b). Single FNPs could be readily tracked over 500 frames with an average localization precision of 4 nm, whereas no significant photobleaching of the FNPs was observed within this observation time (see Figure S9 in the Supporting Information). Single trajectory analysis for mobile FNPs revealed inhomogeneous diffusion alternating between free and highly confined diffusion (Figure 4c,d). For free diffusion, an average diffusion constant of around $0.03\ \mu m^2 s^{-1}$ was obtained. This diffusion constant is significantly lower compared to diffusion constants obtained for TOM7 by fluorescence recovery after photobleaching experiments (around $0.7\ \mu m^2 s^{-1}$).[18] However, the extended confinement periods suggest that diffusion may be affected by steric hindrance because of the size of the FNPs, which requires further investigation.

In summary, we here report for the first time a generic method for specific and efficient targeting of nanoparticles to fusion proteins in the cytoplasm of cells. Nanoparticle targeting was achieved by increasing the rate constant of an enzymatic reaction and by using FNPs with reduced nonspecific interactions. Our results indicate that specific intracellular nanoparticle targeting requires a minimum ratio between the rate constants of nonspecific versus specific interactions. Thus, we succeeded to track the diffusion of individual proteins in the membrane of an organelle with a localization precision of a few nanometers. This approach can be adapted to other types of nanoparticles and will considerably extend the application of nanoparticles towards probing protein functions and dynamics in the cytoplasm and on the surface of intracellular membranes.

Received: March 1, 2011
Revised: June 14, 2011
Published online: August 22, 2011

Keywords: click chemistry · fluorescence spectroscopy · nanoparticles · proteins

[1] D. Marguet, P. F. Lenne, H. Rigneault, H. T. He, *EMBO J.* **2006**, *25*, 3446.
[2] F. Pinaud, S. Clarke, A. Sittner, M. Dahan, *Nat. Methods* **2010**, *7*, 275.
[3] M. Dahan, S. Levi, C. Luccardini, P. Rostaing, B. Riveau, A. Triller, *Science* **2003**, *302*, 442.
[4] D. S. Lidke, P. Nagy, R. Heintzmann, D. J. Arndt-Jovin, J. N. Post, H. E. Grecco, E. A. Jares-Erijman, T. M. Jovin, *Nat. Biotechnol.* **2004**, *22*, 198.
[5] X. Michalet, F. F. Pinaud, L. A. Bentolila, J. M. Tsay, S. Doose, J. J. Li, G. Sundaresan, A. M. Wu, S. S. Gambhir, S. Weiss, *Science* **2005**, *307*, 538.
[6] C. Bouzigues, M. Morel, A. Triller, M. Dahan, *Proc. Natl. Acad. Sci. USA* **2007**, *104*, 11251.
[7] M. Howarth, K. Takao, Y. Hayashi, A. Y. Ting, *Proc. Natl. Acad. Sci. USA* **2005**, *102*, 7583.
[8] Y. P. Chang, F. Pinaud, J. Antelman, S. Weiss, *J. Biophotonics* **2008**, *1*, 287.
[9] S. Kim, M. G. Bawendi, *J. Am. Chem. Soc.* **2003**, *125*, 14652.
[10] A. P. Alivisatos, W. Gu, C. Larabell, *Annu. Rev. Biomed. Eng.* **2005**, *7*, 55.
[11] W. Liu, M. Howarth, A. B. Greytak, Y. Zheng, D. G. Nocera, A. Y. Ting, M. G. Bawendi, *J. Am. Chem. Soc.* **2008**, *130*, 1274.
[12] C. You, S. Wilmes, O. Beutel, S. Lochte, Y. Podoplelowa, F. Roder, C. Richter, T. Seine, D. Schaible, G. Uze, S. Clarke, F. Pinaud, M. Dahan, J. Piehler, *Angew. Chem.* **2010**, *122*, 4202; *Angew. Chem. Int. Ed.* **2010**, *49*, 4108.
[13] G. V. Los, L. P. Encell, M. G. McDougall, D. D. Hartzell, N. Karassina, C. Zimprich, M. G. Wood, R. Learish, R. F. Ohana, M. Urh, D. Simpson, J. Mendez, K. Zimmerman, P. Otto, G. Vidugiris, J. Zhu, A. Darzins, D. H. Klaubert, R. F. Bulleit, K. V. Wood, *ACS Chem. Biol.* **2008**, *3*, 373.
[14] M. K. So, H. Yao, J. Rao, *Biochem. Biophys. Res. Commun.* **2008**, *374*, 419.
[15] M. Gavutis, S. Lata, P. Lamken, P. Müller, J. Piehler, *Biophys. J.* **2005**, *88*, 4289.
[16] S. Lata, J. Piehler, *Anal. Chem.* **2005**, *77*, 1096.
[17] J. Riedl, A. H. Crevenna, K. Kessenbrock, J. H. Yu, D. Neukirchen, M. Bista, F. Bradke, D. Jenne, T. A. Holak, Z. Werb, M. Sixt, R. Wedlich-Soldner, *Nat. Methods* **2008**, *5*, 605.
[18] V. M. Sukhorukov, D. Dikov, K. Busch, V. Strecker, I. Wittig, J. Bereiter-Hahn, *Biochim. Biophys. Acta Biomembr.* **2010**, *1798*, 2022.

